ELSEVIER

Contents lists available at ScienceDirect

## Electrochimica Acta

journal homepage: www.journals.elsevier.com/electrochimica-acta





## Fabrication of electrochemical sensor based on Eu<sub>2</sub>O<sub>3</sub>/rGO nanostructure for endocrine disruptor estradiol sensing. Theoretical perspective on the sensing mechanism

Aleksandar Mijajlović <sup>a</sup>, Vesna Stanković <sup>b</sup>, Filip Vlahović <sup>b</sup>, Tijana Mutić <sup>b</sup>, Petar Ristivojević <sup>a</sup>, Nikolaos Argirusis <sup>c</sup>, Georgia Sourkouni <sup>d</sup>, Christos Argirusis <sup>c</sup>, Jasmina Vidić <sup>f</sup>, Dalibor Stanković <sup>a</sup>, <sup>\*</sup>

- <sup>a</sup> Department of Analytical Chemistry, Faculty of Chemistry, University of Belgrade, Studentski trg 12-16 11000, Belgrade, Serbia
- b Department of Chemistry, Institute of Chemistry, Technology and Metallurgy, University of Belgrade, Njegoševa 12 11000, Belgrade, Serbia
- c mat4nrg GmbH, Burgstätterstr. 42, 38678 Clausthal-Zellerfeld, Germany
- d Clausthal Center of Materials Technology, Technische Universität Clausthal, Leibnizstr. 9, 38678 Clausthal-Zellerfeld, Germany
- e Laboratory of Inorganic Materials Technology (LIMT), School of Chemical Engineering, National Technical University of Athens (NTUA), I. Polytechniou 9, 15773 Zografou/Athens, Greece
- <sup>f</sup> Université Paris-Saclay, INRAE, AgroParisTech, Micalis Institute, 78350 Jouy en Josas, France

## ARTICLE INFO

# Keywords: Rare earth element Endocrine disruptor Voltammetry Electrochemical sensor Density functional theory

## ABSTRACT

Accurate detection and monitoring of endocrine disruptor estradiol in clinical and environmental contexts are crucial due to its implications for health and ecological systems. In this work, we developed an electrochemical sensor based on europium oxide (Eu<sub>2</sub>O<sub>3</sub>) and reduced graphene oxide (rGO) for quantification of estradiol in aqueous solutions. Eu<sub>2</sub>O<sub>3</sub> synthesized using the hydrothermal method formed ultrasmall and uniform nanoparticles and showed an efficient electrochemical behavior. Eu<sub>2</sub>O<sub>3</sub> nanoparticles were incorporated with rGO and characterized by XRD, FTIR, SEM, and TEM. The obtained Eu<sub>2</sub>O<sub>3</sub>@rGO composite was drop-casted on the surface of a screen-printed carbon electrode to construct a sensor for estradiol quantification. The fabricated sensor exhibited an impressive limit of detection (0.06  $\mu$ M) and a limit of quantification (0.236  $\mu$ M), with a sensitivity of 2.44  $\mu$ A  $\mu$ M<sup>-1</sup> cm<sup>-2</sup>, using SWV. The obtained SWV curve shows the oxidation current increased during the addition of estradiol concentration from 0.1 to 30  $\mu$ M. The practical applicability of the SPCE/Eu<sub>2</sub>O<sub>3</sub>@rGO sensor was demonstrated for detecting estradiol in tap water, river water, and saliva samples. The results obtained with the SPCE/Eu<sub>2</sub>O<sub>3</sub>@rGO sensor closely matched those from the UV–Vis validation method, confirming its reliability and accuracy. The developed sensor represents a promising candidate for routine environmental analysis due to its portability, lower cost, and potential for on-site and real-time monitoring.

## 1. Introduction

Estradiol (E2), the foremost estrogen hormone, regulates reproductive and non-reproductive physiological processes in humans and animals. As a major estrogen, estradiol helps the formation and maintenance of female reproductive tissues, bone density, and cardio-vascular health [1]. Besides, estradiol is a biomarker for several illnesses in human health, such as infertility, and hormone-related malignancies. Hormone-sensitive cancers, including ovarian and breast cancer, or endocrine problems may be indicated by abnormal estradiol levels

[2–3]. Beyond its biomedical relevance, estradiol is increasingly recognized as an emerging environmental contaminant due to its classification as an endocrine-disrupting compound, capable of altering endocrine functions in both animals and humans. It primarily enters aquatic ecosystems through wastewater discharge, encompassing effluents from pharmaceutical manufacturing, healthcare facilities, and agricultural runoff containing animal waste. The presence of estradiol in aquatic environments presents significant risks to aquatic life, particularly by disrupting reproductive processes, which may result in reduced fertility and ecological imbalances. Therefore, rigorous monitoring of

E-mail address: dalibors@chem.bg.ac.rs (D. Stanković).

<sup>\*</sup> Corresponding author.

estradiol levels in water systems is essential to mitigate potential environmental and ecological hazards [4–5]. Conventional methods for detecting estradiol, including high-performance liquid chromatography (HPLC) and enzyme-linked immunosorbent assays (ELISA), provide excellent sensitivity and specificity. However, these techniques are often associated with high costs, lengthy analysis times, and intricate sample preparation procedures [6]. Therefore, a new, accurate, rapid, and affordable method for the detection and monitoring of estradiol in clinical and environmental samples is urgently needed for health and environmental applications.

In recent years, sensor-based technologies have gained significant attention as a promising alternative for estradiol detection, offering rapid, cost-efficient, and on-site monitoring capabilities. The advancement of innovative sensors aims to overcome the drawbacks of traditional techniques while improving the effectiveness of monitoring in diverse matrices such as biological fluids and environmental water sources [7]. Because of their unique electrical, optical, and catalytic properties, rare-earth metal oxides have piqued the curiosity of electrochemists. Their exceptional stability and great electrical conductivity make them ideal for electrochemical sensors and systems. Notably, rare-earth oxides can improve electron transport kinetics at electrode surfaces, increasing sensitivity while decreasing response time in electrochemical systems. Including these materials into electrochemical systems shows great potential for real-time monitoring and detection, especially in environmental and medicinal applications [8–9].

 $Eu_2O_3$  was selected due to its favorable electrocatalytic and surface properties. Europium stands out among lanthanides for its pronounced redox behavior and catalytic potential. The surface of  $Eu_2O_3$  contains a variety of reactive sites that enhance both adsorption and catalysis. Importantly,  $Eu_2O_3$  remains stable in the  $Eu^{3+}$  oxidation state under typical sensing conditions, while its inherent oxygen vacancies (structural defects) can act as active sites for analyte adsorption and facilitate electron and proton transfer during redox reactions [10–12]. These characteristics contribute to richer surface chemistry compared to many conventional metal oxides, ultimately improving both the activity and selectivity of the sensor. For phenolic analytes such as estradiol, this translates into enhanced molecular recognition and a stronger electrochemical signal.

Reduced graphene oxide (rGO) has become a compelling material in electrochemistry, primarily due to its outstanding electrical conductivity, expansive surface area, and abundance of surface functional groups. Its distinctive structure—comprising several layers of  $sp^2$ -hybridized carbon atoms interspersed with residual oxygen-containing groups—offers a high density of active sites for electrochemical reactions. Moreover, the large surface area of rGO enhances the electrode's ability to adsorb analytes, thereby improving detection sensitivity and selectivity [13–14].

In this study, estradiol was detected for the first time using a modified screen-printed carbon electrode (SPCE)with  $Eu_2O_3$  nanoparticles and rGO composite. The synergistic combination of  $Eu_2O_3$  and rGO in the SPCE/Eu<sub>2</sub>O<sub>3</sub>@rGO sensor enhances electrochemical performance by integrating the excellent conductivity and high surface area of rGO with the redox activity of  $Eu_2O_3$ . This interaction improves electron transfer, analyte adsorption, and overall sensor sensitivity, making it a highly effective platform for E2 detection in environmental and biomedical applications. The method demonstrated high selectivity and sensitivity in detecting E2 in water and human saliva samples, with results validated with the standard UV/Vis method.

## 2. Experimental

## 2.1. Chemicals and instrumentation

## 2.1.1. Materials

Europium (III) nitrate pentahydrate (Eu(NO<sub>3</sub>)<sub>3</sub> x  $5H_2O$ ), sodium hydroxide (NaOH), potassium ferrocyanide (K<sub>4</sub>[Fe(CN)<sub>6</sub>]), potassium

ferricyanide ( $K_3[Fe(CN)_6]$ ), potassium chloride (KCl), sodium sulfide ( $Na_2S$ ), graphene oxide (GO), potassium hydroxide (KOH), potassium chloride (KCl), sodium nitrite ( $NaNO_2$ ), sodium nitrate ( $NaNO_3$ ), calcium chloride ( $CaCl_2$ ), magnesium chloride ( $MgCl_2$ ), dopamine, ascorbic acid, uric acid, caffeine, threonine and estradiol were obtained from Sigma-Aldrich and directly used for the experimental investigations without purification.

Britton–Robinson buffer solution (BRBS) was prepared as a supporting electrolyte by mixing equimolar amounts of phosphoric, acetic, and boric acids (40 mM). NaOH solution (0.2 M) was used for adjusting the pH values of the buffer. A pH meter equipped with a universal glass electrode (Orion 1230, Thermo Fisher Scientific, Waltham, Massachusetts, USA) was used for all pH measurements. For the preparation of all solutions, double-distilled water was used.

## 2.1.2. Electrochemical investigations

For electrochemical measurements (cyclic voltammetry (CV), square wave voltammetry (SWV)), the potentiostat/galvanostat PalmSens, model 4 (PalmSens BV, Vleugelboot 22, 3991 CL Houten The Netherlands) was used. A classical three-electrode system with a (un) modified SPCE as the working electrode (WE), a platinum plate as a counter electrode (CE), and Ag/AgCl (3 M KCl) as a reference electrode (RE) was used.

## 2.1.3. IR-spectroscopy and XRD analysis

After the visual impression and the analysis of the products based exclusively on the product yield, the powders were analyzed using both infrared spectroscopy (IR) and powder diffraction (XRD). The Alpha-T IR device, manufactured by BRUKER®, was employed for IR spectroscopy. Before commencing the measurements, the ATR crystal of the device was subjected to a cleaning process. Subsequently, approximately 5 mg of the synthesized powder was positioned on the crystal and pressed onto it using a stamp. The recorded values were obtained at wavenumbers ranging from 4000 cm<sup>-1</sup> to 400 cm<sup>-1</sup> with a step size of approximately 2,06 cm<sup>-1</sup>.

The powder diffraction experiments were conducted using devices manufactured by Panalytical. The samples were analyzed on two distinct devices manufactured by the same company, both of which were of the Empyrean type. A Cu Ka X-ray source (wavelengths: Ka1 = 1, 5405,980 Å, Ka2 = 1, 5444,260 Å) and a PIXcel1D detector (Panalytical) with 255 measuring channels were used. The XRD measurement was carried out in the angular range from  $10^\circ$  to  $90^\circ$  with a step size of  $0.0262.606^\circ$ 

## 2.1.4. SEM and TEM analysis

Scanning electron microscopy (SEM) imaging and energy dispersive X-ray spectroscopy (EDXS) were performed using a FEI Helios NanoLab 660 SEM/FIB dual-beam system.

A JEOL JEM 2100 microscope was utilized for TEM investigation, operating at an accelerating voltage of  $120~\rm kV$  for all measurements. To prepare the sample, a TEM grid was positioned in a snap-lid jar containing the powder for analysis. The powder was subsequently agitated to facilitate its deposition onto the grid. The biggest particles were eliminated by agitating the sample outside the snap-lid container.

## 3. Materials preparation

Synthesis of Eu<sub>2</sub>O<sub>3</sub> nanoparticles—The nanoparticles of Eu<sub>2</sub>O<sub>3</sub> were synthesized using the hydrothermal method, following literature procedure with minor modification [15]. The first solution was prepared by dissolving 4  $\times$  10<sup>-4</sup> mol (0.1941 g) of Eu(NO<sub>3</sub>)<sub>3</sub> x 5H<sub>2</sub>O in 1 mL of distilled water. A second solution was prepared by dissolving 1.68 g of NaOH in 7 mL of distilled water (to obtain a 6 M solution), and these two solutions were mixed at room temperature and stirred for 30 min. After the formation of the milky slurry, the reaction mixture was transferred to a stainless-steel vessel autoclave for 24 h at 100 °C. After cooling to

room temperature, the precipitate was centrifuged and washed three times with distilled water and ethanol. Finally, the product was calcinated for 6 h at 450 °C. To modify the electrode, a suspension of Eu<sub>2</sub>O<sub>3</sub> in DMF was prepared with a concentration of 1 mg/mL. The suspension was subjected to ultrasonic treatment for 1 hour, after which it was ready for use.

Synthesis of rGO – The synthesis of rGO was carried out according to the referenced procedure, using ten times smaller amounts of reagents [16]. Briefly, 0.3 g of graphite was added to 7 mL of concentrated sulfuric acid under continuous stirring at room temperature. Afterward, 0.15 g of sodium nitrate was introduced, and the mixture was cooled to 0 °C. Under vigorous stirring, 0.9 g of potassium permanganate was gradually added, ensuring the reaction temperature remained below 20 °C. The mixture was then transferred to a water bath at 35-40 °C and maintained for 30 min, forming a dense paste. Subsequently, 14 mL of water was added, and the system was stirred for an additional 15 min, followed by dilution with 50 mL of water and the slow addition of 2 mL of hydrogen peroxide (30 %), which turned the mixture from brown to vellow. The product was filtered and washed sequentially with 25 mL of 1:10 diluted hydrochloric acid and deionized water, then centrifuged repeatedly to eliminate residual acids. The obtained solid was redispersed in water using ultrasonication for 1 hour to yield a 0.5 wt % GO suspension. The dispersion was centrifuged at 4000 rpm for 30 min to remove aggregates and further purified by dialysis for 7 days to eliminate residual salts. For reduction to rGO, 0.1-0.2 mg/mL GO aqueous suspensions were prepared, to which Na<sub>2</sub>S solution (5.4 mmol/L) was added. The mixture was then heated at 90 °C for 3 h without stirring. The resulting graphene hydrogel was thoroughly washed with deionized water and ethanol to remove unreacted components and residual salts.A suspension of rGO in DMF was prepared for easier modification of working electrodes, with a final concentration of 1 mg/ml.The suspension was subjected to ultrasonic treatment for 1 hour and was subsequently ready for use. A suspension of rGO in DMF was prepared for easier modification of working electrodes, with a final concentration of 1 mg/ml. The suspension was subjected to ultrasonic treatment for 1 hour and was subsequently ready for use.

Fabrication of Eu<sub>2</sub>O<sub>3</sub>@rGO nanocomposite – To synthesize the Eu<sub>2</sub>O<sub>3</sub>/rGO composite, 0.5 mg of np-Eu<sub>2</sub>O<sub>3</sub> was mixed with 0.5 mg of rGO and dissolved in DMF, resulting in a final composite concentration of 1 mg/ml. The composite was subjected to ultrasonic treatment for 2 h to facilitate the incorporation of nanoparticles into the rGO structure.

## 4. Electrode modification

Before each electrochemical measurement, every individual SPCE was activated using an identical procedure. The electrodes underwent cyclic voltammetry in 0.1 M  $\rm H_2SO_4$  at a scan rate of 100 mV  $\rm s^{-1}$  for 50 cycles to enhance surface functionality and remove impurities.

To compare the electrocatalytic properties of the synthesized materials and composites, four working electrodes were prepared with the following labels: SPCE, SPCE/Eu<sub>2</sub>O<sub>3</sub>, SPCE/rGO, and SPCE/Eu<sub>2</sub>O<sub>3</sub>@rGO. The working electrodes were modified by applying different amounts of material. For each material intended for SPCE modification, a dispersion was prepared in DMF at a final concentration of 1 mg/mL. Subsequently, aliquots of 2.5, 5, and 10  $\mu L$  were drop-cast onto the working area of the SPCEs and left to dry overnight under ambient conditions to ensure complete solvent evaporation prior to use.

## 4.1. Preparation of standard curve for the UV method

A parallel analysis of real samples was conducted using spectrophotometric measurements to validate the application of the proposed electroanalytical method. The analysis was performed with minor modifications to the referenced procedure [17]. The wavelength selected for E2 detection was 280.75 nm. The calibration curve was prepared from a standard stock solution of E2 by dissolving an appropriate amount of E2 in methanol. From this stock, standard working solutions were obtained to achieve final concentrations of 4–20  $\mu$ M in 10 mL volumetric flasks by appropriate dilution.

## 4.2. Preparation of the real sample

The proposed SPCE/Eu<sub>2</sub>O<sub>3</sub>@rGO sensor and the developed electroanalytical method were employed to determine E2 in tap water, river water, and human saliva samples. Tap water samples were collected in Belgrade, Serbia, and stored at 4 °C in a refrigerator prior to analysis. Before the measurements, the samples were diluted tenfold with BRBS solution (pH = 4) and analyzed directly. River water was sampled from the Danube River (Zemun, Serbia) and similarly stored at 4 °C. Before electroanalytical measurements, the samples were centrifuged at 5000 rpm for 5 min to remove suspended particles, and the filtrate was further passed through a 0.45 µm filter. The processed samples were then diluted tenfold with BRBS solution (pH = 4) and analyzed directly. Saliva samples were gathered from two healthy volunteers (one male and one female) at least one hour post-meal after thoroughly rinsing their mouths with water. The samples were collected in 1.5-mL tubes and stored at -20 °C until further use. Sample preparation for electrochemical testing involved centrifugation at 5000 rpm for 30 min, filtration through a 0.45 µm filter, and subsequent tenfold dilution with BRBS solution (pH = 4). For spectrophotometric analysis, the samples were prepared in the same manner.

## 5. Results and discussion

### 5.1. Structural analysis

Fig. 1 show SEM micrographs of the used not yet exfoliated (prior to sonication) rGO (A), the prepared Eu<sub>2</sub>O<sub>3</sub> powder (B) and of the Eu<sub>2</sub>O<sub>3</sub>@rGO composite material (C). Fig. 1C demonstrates the successful formation of the Eu<sub>2</sub>O<sub>3</sub>@rGO composite, where Eu<sub>2</sub>O<sub>3</sub> nanorods are evenly distributed and well-adhered to the rGO matrix, indicating good dispersion and interaction. The Eu<sub>2</sub>O<sub>3</sub> particles exhibit an elongated form with a length of 300–1000 nm and a thickness of 50–100 nm (Fig. 1D). Fig. 1E and F illustrate the intimate contact between Eu<sub>2</sub>O<sub>3</sub> and the exfoliated rGO nanosheets. The Eu<sub>2</sub>O<sub>3</sub> rods are clearly anchored onto single rGO sheets, which supports good interfacial adhesion and suggests favorable electron transfer properties.

The FT-IR spectrum of GO exhibits characteristic peaks at  $\sim$ 1720 cm<sup>-1</sup> (C=O stretching),  $\sim$ 1220 cm<sup>-1</sup> (C-O-C stretching), and broad -OH vibrations in the 3200–3400 cm<sup>-1</sup> range, confirming the presence of oxygen-containing functional groups. Upon reduction to rGO, these bands significantly decrease in intensity, indicating successful deoxygenation. The spectrum of Eu<sub>2</sub>O<sub>3</sub> shows a strong absorption band near 545 cm<sup>-1</sup>, corresponding to Eu $_2$ O vibrations. In the composite material (Eu<sub>2</sub>O<sub>3</sub>@rGO), both Eu $_2$ O bands and residual oxygen functionalities from rGO are present, suggesting successful integration of metal oxide onto the carbon surface, while preserving key vibrational features. These observations confirm the formation of a stable hybrid structure [17 $_2$ 18]

The XRD diffractogram (Fig. 2B) shows all major Eu $_2$ O $_3$  peaks compared to the reference as deposited at the International Centre for Diffraction Data (ICDD database record no 00–034–0392) with some small additional peaks between 20 and 30 ° The XRD pattern of Eu $_2$ O $_3$  corresponds well with the standard ICDD database record no 00–034–0392, confirming the cubic crystalline phase with space group Ia-3 (no. 206). The most intense peak at  $2\theta \approx 28.43^\circ$  is assigned to the (222) reflection, with a calculated interplanar spacing (d) of 3.137 Å using Bragg's law. These results are consistent with values obtained from TEM images of the composite (Fig. 1F), where the lattice fringe distance is also around 0.31 nm.

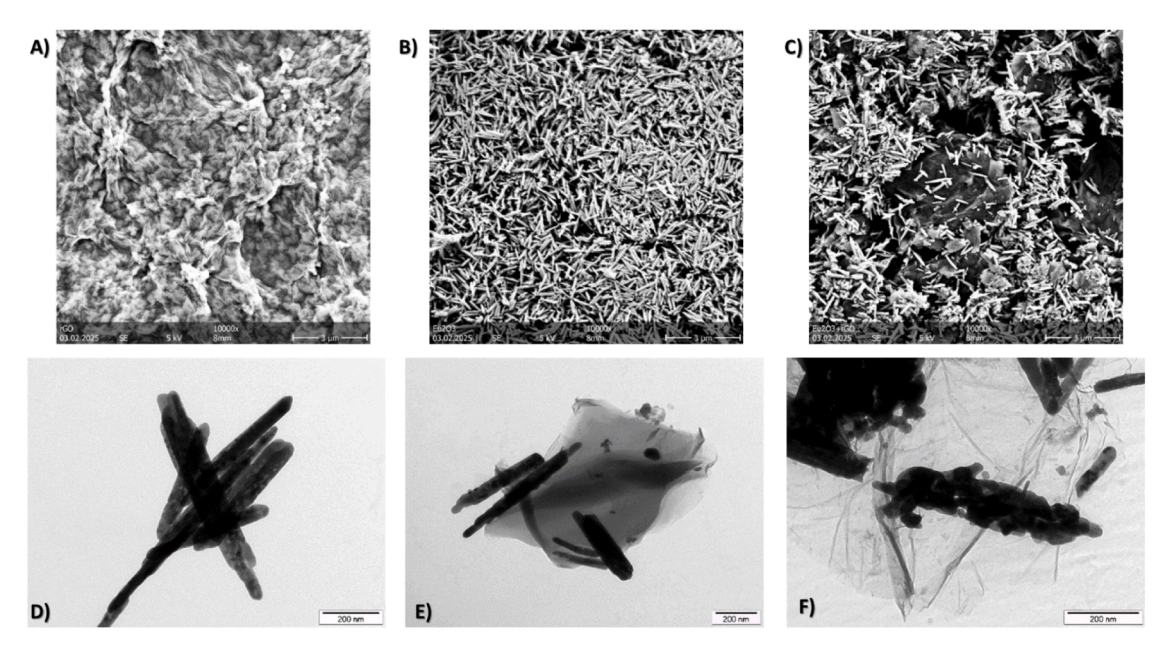


Fig. 1. SEM micrographs of A) the used not yet exfoliated rGO (prior to sonication), B) the prepared  $Eu_2O_3$  powder and C) of the  $Eu_2O_3$ @rGO composite material; TEM pictures of D)  $Eu_2O_3$  powder E)  $Eu_2O_3$ @rGO and F) magnification of  $Eu_2O_3$ @rGO.

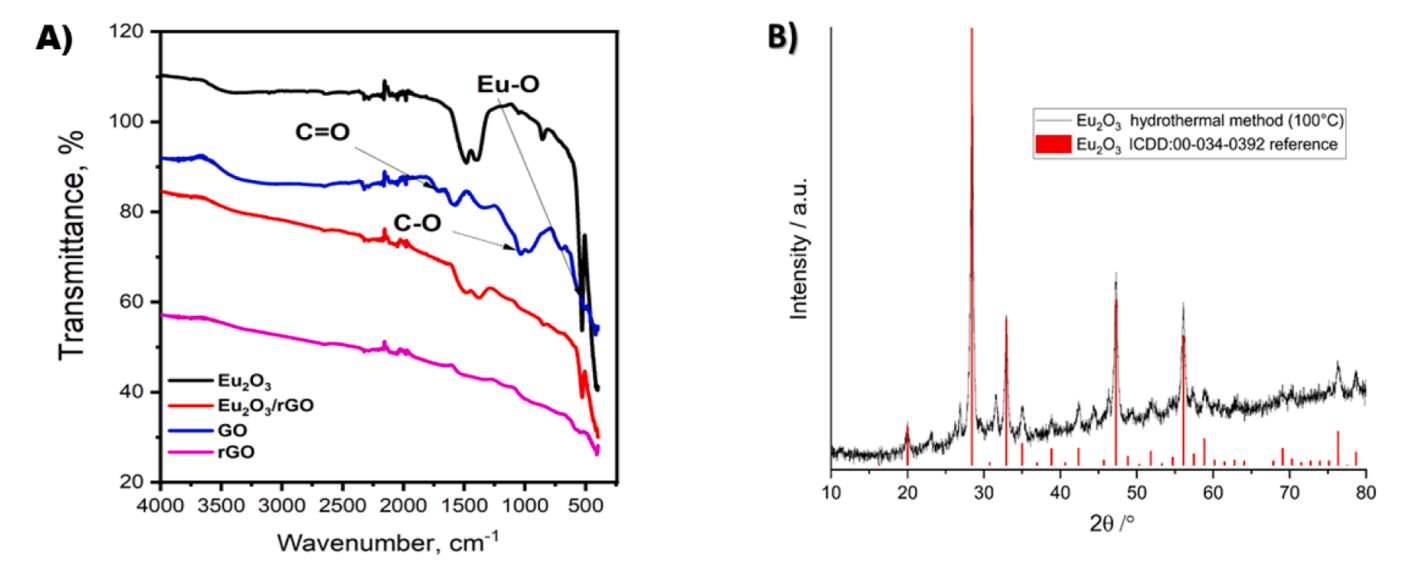


Fig. 2. A) FT-IR spectrum of the pristine  $Eu_2O_3$  powder; B) XRD patterns of  $Eu_2O_3$  powder and the reference material as deposited at the International Centre for Diffraction Data (ICDD database record no 00-034-0392).

## 6. Exploring electrochemical insights

The main objective of this study was to develop an SPCE/  $Eu_2O_3@rGO$  sensor for the detection of E2 in water samples.

## 6.1. Optimization of nanocomposite amount added to SPCE

Optimization of the amount of nanocomposite added to the SPCE was performed by cyclic voltammetry. In this experiment, the electrochemical responses of SPCEs modified with 2.5  $\mu L$ , 5  $\mu L$ , and 10  $\mu L$  of 1 mg mL $^{-1}$  Eu<sub>2</sub>O<sub>3</sub>, rGO, and Eu<sub>2</sub>O<sub>3</sub>@rGO nanocomposite were compared. The effect of the amount of added material on the working electrode was investigated in a solution of 5 mM [Fe(CN)<sub>6</sub>] $^{3-/4-}$  in 0.1 M KCl at a scan rate of 50 mV s $^{-1}$ .

Based on the obtained results presented in Figure S1, it was concluded that the optimal amount is 10  $\mu L$  for SPCE/ rGO, 5  $\mu L$  for SPCE/Eu<sub>2</sub>O<sub>3</sub>,

and 2.5  $\mu L$  for the composite. Further electrochemical investigations were conducted using the specified quantities of the modified SPCEs.

## 6.2. Evaluating the electrocatalytic efficiency of working electrodes

The electrocatalytic properties of the modified electrodes were analyzed using electrochemical impedance spectroscopy (EIS) in a 0.1 M KCl solution containing 5 mM [Fe(CN)<sub>e</sub>]<sup>3-/4</sup>. Measurements were performed at a potential of 0 V, with a frequency range spanning from 0.01 Hz to 100 kHz. The resulting impedance data were modeled using the Randles equivalent circuit, as illustrated in the inset of Fig. 3A, where  $R_{\rm ct}$  denotes charge transfer resistance,  $R_{\rm s}$  indicates electrolyte resistance,  $Z_{\rm w}$  corresponds to Warburg impedance, and  $C_{\rm dl}$  represents double-layer capacitance. The semicircular part of the Nyquist plot illustrates the charge transfer limitations, whereas the extended linear region reflects the diffusion-limited process. The diameter of the semicircle is typically

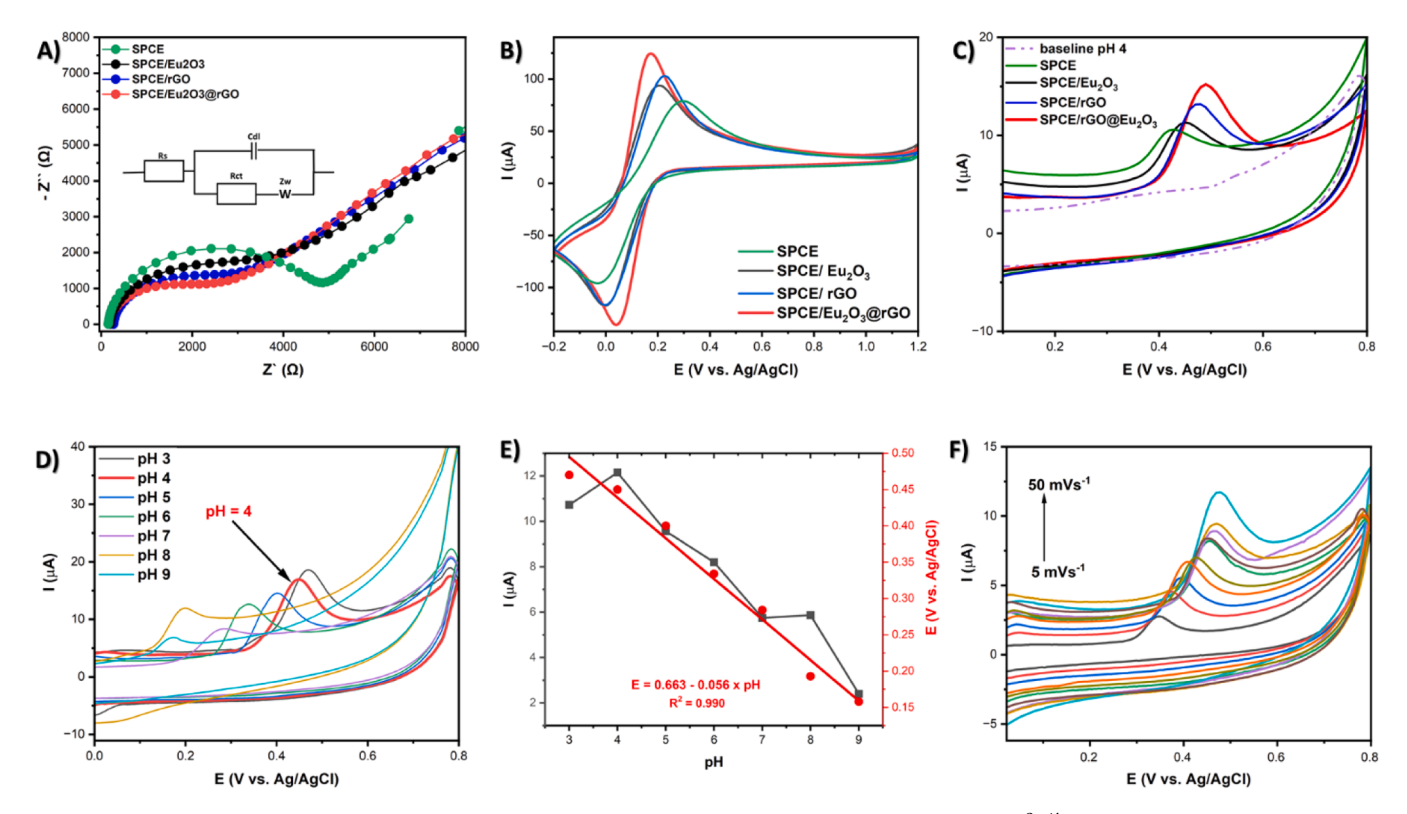


Fig. 3. A) EIS spectra of bare SPCE; SPCE@rGO; SPCE/Eu<sub>2</sub>O<sub>3</sub>; SPCE/ rGO@Eu<sub>2</sub>O<sub>3</sub> in redox probe of 5 mM [Fe(CN)6]<sup>3-/4-</sup> in 0.1 M KCl solution. (Inset: Randles Equivalent circuit image); B) CV response of bare SPCE; SPCE@rGO; SPCE/Eu<sub>2</sub>O<sub>3</sub>; SPCE/rGO@Eu<sub>2</sub>O<sub>3</sub> at a scan rate 50 mV s<sup>-1</sup>; C) CV response of SPCE/rGO@Eu<sub>2</sub>O<sub>3</sub> at different pH (3.0–9.0) of BRBS at a scan rate 50 mV s<sup>-1</sup>; D) The corresponding linear plot for different pH (3.0–9.0) versus potential and current; E) CV response of SPCE/rGO@Eu<sub>2</sub>O<sub>3</sub> in 100 μM of E2 at different scan rates (5–50 mV s<sup>-1</sup>) in BRBS at pH 4.0.

used to quantify the electrode's charge transfer resistance. The recorded Rct values were 4870  $\Omega$ , 3434  $\Omega$ , 2699  $\Omega$ , and 2313  $\Omega$  for SPCE, SPCE/Eu<sub>2</sub>O<sub>3</sub>, SPCE/rGO, and SPCE/Eu<sub>2</sub>O<sub>3</sub>@rGO, respectively. The results indicate that the composite material successfully reduced the electron transfer resistance by 2.105 times, which can be explained by the synergistic properties of Eu<sub>2</sub>O<sub>3</sub>, such as its high surface-to-volume ratio, ultra-small particle size, and the enhanced number of adsorptive sites provided by rGO, which significantly increases the active surface area. Therefore, the novel composite is a highly promising material for electrochemical sensing applications. Furthermore, a charge transfer rate (Ks) was determined using the following Equation (Eq.). 1:

$$Ks = \frac{RT}{n^2 F^2 R_{ct} C} \tag{1}$$

where R is the universal gas constant (8.314 J mol $^{-1}$  K $^{-1}$ ), T is the temperature of the reaction, n is the number of the electrons transferred in the reaction, F is Faraday's constant (96,485 C mol $^{-1}$ ), and C represents the concentration of the redox couple. Calculated Ks values are  $1.09\times10^{-8} \text{cm s}^{-1}$ ,  $1.55\times10^{-8} \text{ cm s}^{-1}$ ,  $1.97\times10^{-8} \text{ cm s}^{-1}$ , and  $2.30\times10^{-8} \text{ cm s}^{-1}$  for SPCE, SPCE/Eu<sub>2</sub>O<sub>3</sub>, SPCE/ rGO, and SPCE/Eu<sub>2</sub>O<sub>3</sub>@rGO, respectively. These values demonstrate that Ks increases as Rct decreases, which is expected since lower resistance indicates faster charge transfer. This further confirms the enhanced electrocatalytic response of the newly synthesized material [19].

The electrocatalytic performance of the modified electrode was further examined through cyclic voltammetry (CV) in a 0.1 M KCl solution containing 5 mM [Fe(CN)<sub>6</sub>]<sup>3-/4-</sup> as the redox probe (Fig. 3B). The measurements were conducted at a scan rate of 50 mV s<sup>-1</sup> within a potential range of -0.2 to 1.0 V. When compared to the bare SPCE, the modified electrodes exhibited the greater redox peak current value in the observation of the CV findings. Compared to other electrodes (SPCE, SPCE/rGO, SPCE/Eu<sub>2</sub>O<sub>3</sub>), SPCE/Eu<sub>2</sub>O<sub>3</sub>@rGO exhibits a notably smaller

redox peak separation ( $_{\Delta}$ Ep) of 135 mV, along with a higher current response. In contrast, the redox peak separations for the other modified electrodes are SPCE (267 mV), SPCE/Eu<sub>2</sub>O<sub>3</sub> (233 mV), and SPCE/rGO (210 mV).

The impact of the mentioned synergy on the electrocatalytic activity of this material was additionally clarified by the calculation of the electroactive surface area (EASA). Figure S2. depicts scan rate (10–200 mV s<sup>-1</sup>) examinations of bare SPCE, SPCE/Eu<sub>2</sub>O<sub>3</sub>, SPCE/rGO, and SPCE/Eu<sub>2</sub>O<sub>3</sub>@rGO in 5 mM [Fe(CN)<sub>6</sub>]<sup>3-/4-</sup> solution. The linear correlation was obtained between the current and the square root of the scan rate. EASA of all working electrodes was calculated using Randles-Sevcik Eq. (2) [20]:

$$Ip = (2.69 \times 10^5) \times A \times n^{2/3} \times D^{1/2} \times C \times v^{1/2}$$
(2)

where A denotes the electroactive surface area of the electrode, n is the number of transferred electrons, D represents the diffusion coefficient, V is the scan rate, and Ip depicts the peak current. The EASA values for SPCE, SPCE/Eu<sub>2</sub>O<sub>3</sub>, SPCE/rGO, and SPCE/Eu<sub>2</sub>O<sub>3</sub>@rGO were calculated to be 0.0373, 0.0436, 0.0454, and 0.05173 cm², respectively. These results indicate that SPCE/Eu<sub>2</sub>O<sub>3</sub>@rGO exhibits the highest EASA value among the modified electrodes. The larger surface area of the proposed SPCE/Eu<sub>2</sub>O<sub>3</sub>@rGO nanocomposite, which offered an enhanced electrode–electrolyte interface for the accumulation of charged species and improved electron transferability, was the primary cause of the higher redox current response of SPCE/Eu<sub>2</sub>O<sub>3</sub>@rGO during electrocatalysis.

Determining the heterogeneous rate constant ( $j_o$ ) is of critical importance in electrochemical studies of materials, as it provides valuable insight into the intrinsic kinetics of electron transfer at the electrode/electrolyte interface [21]. The exchange current density ( $j_o$ ) of the reaction was calculated using the following Eq. (3):

$$jo = \frac{RT}{nFARct} \tag{3}$$

with already-explained symbols. Additional confirmation of the superior performance of the composite material, compared to the other tested materials, is provided by the calculated jo values (A cm $^{-2}$ ), which are as follows: 141.4  $\mu A$  cm $^{-2}$  for SPCE, 171.5  $\mu A$  cm $^{-2}$  for SPCE/Eu<sub>2</sub>O<sub>3</sub>, 209.6  $\mu A$  cm $^{-2}$  for SPCE/rGO, and 214.6  $\mu A$  cm $^{-2}$  for SPCE/Eu<sub>2</sub>O<sub>3</sub>@rGO.

The calculated effective electrode surface area was utilized to determine the surface coverage and surface concentration of electroactive species on the modified electrode, employing the Brown-Anson Eq. (4) [22]:

$$Ipa = \frac{n^2 F^2 C A \nu}{4RT} \tag{4}$$

where F is the Faraday constant (96,500 C mol<sup>-1</sup>), n is the number of electrons transferred (n=1), A is the electrode surface area, R is the universal gas constant (8.314 J mol<sup>-1</sup> K<sup>-1</sup>), Ip<sub>a</sub> is the oxidation current, C is the surface concentration of the absorbed electroactive species and  $\nu$  is the scan rate (20 mVs <sup>-1</sup>). From this equation, the surface concentrations of electroactive species of the working electrode were evaluated to be  $0.4939 \times 10^{-8}$  mol dm<sup>-2</sup>,  $0.5274 \times 10^{-8}$  mol dm<sup>-2</sup>,  $0.5583 \times 10^{-8}$  mol dm<sup>-2</sup> for SPCE, SPCE/Eu<sub>2</sub>O<sub>3</sub>, SPCE/ rGO, and SPCE/Eu<sub>2</sub>O<sub>3</sub>@rGO, respectively. From this, it can be concluded that SPCE/Eu<sub>2</sub>O<sub>3</sub>@rGO has a high surface area and permits a large degree of coverage by the electroactive species. This could ease the promotion of the mass and ions transportation towards the target.

The SPCE/Eu<sub>2</sub>O<sub>3</sub>@rGO electrode exhibited a low charge transfer resistance (Rct), a high electrochemically active surface area, and an efficient surface concentration of electroactive species. Additionally, the enhanced surface concentration of electroactive species contributed to increased current density toward the target. These features improved the electrocatalytic performance, making SPCE/Eu<sub>2</sub>O<sub>3</sub>@rGO a promising candidate for use as an electrochemical sensor for E2 detection.

## 7. Electrochemical behavior of E2 on the SPCE/Eu $_2$ O $_3$ @rGO sensor

To efficiently detect E2 in water samples using SPCE/Eu<sub>2</sub>O<sub>3</sub>@rGO, it is crucial to investigate the nature of the electrode process on the proposed sensor. For this matter, the working electrodes functionalized by different materials were compared regarding their E2 detection capabilities in buffer solution using the CV method, with a scan rate of 50 mV s<sup>-1</sup> (Fig. 3C). The CV results obtained in 100 μM E2 solution in a BRBS at pH 4 revealed that the unmodified SPCE exhibited the lowest anodic current response ( $I = 2.95 \mu A$ ), which can be attributed to inefficient charge transfer between the working electrode and E2. The incorporation of Eu<sub>2</sub>O<sub>3</sub> nanoparticles, known for their high electron transfer rate and exceptional dielectric properties, significantly enhanced the oxidation peak current ( $I = 4.495 \,\mu\text{A}$ ). In contrast, the electrode modified with rGO demonstrated an increase in the oxidation peak current (I = 6.391 $\mu$ A), which is explained by the expansion of the active surface area. Furthermore, the Eu<sub>2</sub>O<sub>3</sub>@rGO composite material exhibited superior performance due to its remarkable electrocatalytic properties attributed to the large surface area, high electrical conductivity, low Rct, numerous active sites, and efficient charge transport between the electrode and electrolyte interface. This was evidenced by an oxidation current response of  $I = 8.47 \mu A$ , nearly three times higher than the bare SPCE. This enhancement highlights the beneficial impact of Eu<sub>2</sub>O<sub>3</sub>@rGO on electrode performance, likely attributed to the unique properties of the material. The interaction between rGO and Eu<sub>2</sub>O<sub>3</sub> significantly enhances the electrocatalytic properties of the composite. rGO provides a highly conductive network that facilitates rapid electron transfer, while Eu<sub>2</sub>O<sub>3</sub> offers active redox sites for estradiol oxidation. The intimate contact between the two phases, supported by residual defect sites and  $\pi$ – $\pi$  interactions, improves charge transport and analyte adsorption. This synergy results in increased current response, lower overpotential and enhanced sensitivity of the sensor platform.

## 8. Key factors influencing the electrochemical oxidation of E2: pH variations and scan rate analysis

## 8.1. Investigating the impact of pH on electrochemical behavior

The pH value of the supporting electrolyte significantly influences the electrochemical behavior of the analyte, making it an essential parameter in electrocatalytic studies. To investigate this, cyclic voltammetry was performed at pH ranging from 3.0 to 9.0, with a constant sweep rate of 50 mV s $^{-1}$ . The oxidation peak current increases as the pH decreases from 3.0 to 9.0, accompanied by a shift in the oxidation potential towards more negative values (Fig. 3D). The highest current response was detected at pH 4.0, while at pH 9.0, the current diminished, and the potential shift became more pronounced. These variations can be attributed to protonation and deprotonation reactions occurring at lower and higher pH values. Additionally, a strong linear relationship between Ep and pH was observed across the range of pH 3.0 to 9.0 (Fig. 3E), as expressed by the following equation: Epa = 0.663 - 0.056 x pH, with  $R^2 = 0.990$ . The obtained slope value was used in the Nernst equation:

$$Ep = -\left(\frac{0.0591 \, m}{n}\right) pH + b \tag{5}$$

where m and n are the number of protons and electrons, respectively. The slope of the curve, 56 mV, is very close to the theoretical Nernstian slope of 59 mV at 25 °C, suggesting that an equal number of protons and electrons participate in the oxidation of E2 on the SPCE/Eu<sub>2</sub>O<sub>3</sub>@rGO sensor. This observation aligns with previous reports [23–25]. Therefore, pH 4.0 was the optimal pH for the supporting electrolyte solution, providing the highest oxidation peak current, and it was chosen for further studies.

## 8.2. Impact of scan rate on electrochemical performance

The influence of scan rate on the redox peak characteristics of E2 was examined using CV assays to analyze mass transport within the diffusion layer and determine the nature of the associated redox process. The electrochemical behavior of  $100 \mu M$  E2 in BRBS at pH 4 at various scan rates (5–50 mV s<sup>-1</sup>) is depicted in Fig. 3F. When the scan rate was higher than 50 mV s<sup>-1</sup>, the peak shape and reproducibility were poor. The SPCE/Eu<sub>2</sub>O<sub>3</sub>@rGO sensor exhibited a linear increase in current response (Ip<sub>a</sub>) for all redox peaks across the applied scan rate ( $\nu$ ) range. The linearity diagram of scan rate vs current response was shown in Figure S3A. The linear dependence was given by the following equation: I ( $\mu$ A) = 1.79 + 0.068 x V (mVs<sup>-1</sup>) with R<sup>2</sup> = 0.992. These findings suggest that the analyte's electrochemical processes at the electrode surface are predominantly governed by adsorption rather than diffusion. Furthermore, the linear correlation obtained between the log scan rate vs Ep is given in Figure S3B. The linear dependence was given by the following equation: E (V) =  $0.24 + 0.136 \times \log V \text{ (mVs}^{-1}) \text{ with } R^2 =$ 0.990, and it was used to calculate the number of electrons transferred via the Laviron (1979) equation [26]:

$$Ep_a = E^0 + \frac{2.3 R x T}{(1 - \alpha)x n x F}$$
 (6)

Where, R, T, F, n, and  $\alpha$  (0.5 for irreversible process) are represented as universal gas constant, temperature, Faraday constant, number of electrons transferred during the oxidation reaction, and electron transfer coefficient, respectively. Then, Epa and Eo are denoted as anodic current potential, and formal potential was calculated using dependence of the log scan rate on Ep. From the slopes of the equation, the number of electrons transferred (n) can be calculated as  $0.86\approx 1.$ 

A. Mijajlović et al. Electrochimica Acta 537 (2025) 146913

## 9. Theoretical investigation

## 9.1. Computational details

The entirety of the results presented herein were derived using the Gaussian 09 [27] electronic structure program suite (Revision A.02) by using the Density Functional Theory (DFT) methodology [28–29]. The computational analyses were executed utilizing the B3LYP [30–31] density functional approximation in conjunction with the 6–311++ $G^{**}$  [32] orbital basis set for all atoms. In an effort to enhance calculation accuracy, the solvation effects of water have been included using the polarizable conductor continuum model (C-PCM) through the solvent cavity reaction field (SCRF) method [33]. The mentioned computational conditions were applied for full optimization and corresponding theoretical investigation.

## 9.2. Theoretical modeling of the experiment

To elucidate the mechanisms underlying the electrochemical behavior of E2, a theoretical investigation of its redox properties was carried out, beginning from the fully relaxed ground-state electron density. From a theoretical standpoint, oxidation is expected to primarily affect the highest occupied molecular orbital (HOMO), while reduction predominantly involves the lowest unoccupied molecular orbital (LUMO). The structure and spatial distribution of the HOMO, shown in Fig. 4A, together with the spin density of the radical cation following one-electron removal (Fig. 4B), support the assignment of the experimentally observed oxidation peak. This peak is therefore attributed to an oxidation process primarily localized within the aromatic ring of the E2 molecule, ultimately corresponding to the oxidation of the phenolic hydroxyl group.

Fig. 4C presents the plot of the Fukui function [34], illustrating the local reactivity of E2 at each point in space toward nucleophilic attack. The analysis indicates that the region's most susceptible to nucleophilic attack by a water molecule are the *ortho* and *meta* positions of the aromatic ring relative to the hydroxyl group. The computed atomic Fukui indices (Table S1) identify C18 as the most reactive site, suggesting it is the most likely to undergo a nucleophilic attack by  $\rm H_2O$  molecule. This hypothetical reaction, followed by further oxidation, would result in the formation of a quinone-like adduct of E2.

Drawing from the insights garnered through our theoretical investigation, we propose two potential oxidation pathways, as illustrated in

Scheme 1. In both proposed mechanisms, oxidation occurs on the aromatic ring and is initiated by electron removal from the phenolic moiety. In the first and more probable pathway, the phenolic group undergoes irreversible oxidation to a ketone, and a new conjugated system is established. In the alternative mechanism, following the initial oxidation step, a water molecule performs a nucleophilic attack on the aromatic core, forming a catechol-like analogue of E2. This intermediate is subsequently oxidized to a quinone-like derivative of E2. The resulting product would be susceptible to reduction, leading to the regeneration of the catechol adduct. However, the absence of a reduction peak in the experimental voltammogram supports the first oxidation pathway as the more likely and dominant process. The results obtained under the applied experimental conditions (scan rate 5-50 mVs<sup>-1</sup>) indicate the presence of a single anodic peak, corresponding to a two-electron transfer process. This observation implies that the second electron transfer occurs so rapidly following the first that the intermediate species cannot be individually detected. The proposed oxidation mechanism is consistent with previously reported findings [35–36].

## 10. E2 determination using SPCE/Eu<sub>2</sub>O<sub>2</sub>@rGO

Square wave voltammetry (SWV) was selected as the preferred method for E2 determination due to its excellent resolution, high sensitivity and low background currents [37–39]. The method parameters were systematically optimized to achieve a broad calibration range with a maximum slope, ensuring optimal sensitivity for E2 measurement. During the optimization process, each parameter was varied individually while keeping all others constant. The final SWV conditions were determined based on the analyte's well-defined peak shape and maximum peak current, with a pulse amplitude of 20 mV, a frequency of 10 Hz, and a potential step of 8 mV.

The obtained SWV curve shows that the oxidation current increased with the addition of E2 concentration from 0.1 to 30  $\mu M.$  A shift in the oxidation peak potential at higher concentrations was also observed, further confirming the previously mentioned explanation of analyte adsorption on the electroactive surface (Fig. 5A). A linear relationship between the oxidation peak currents and concentrations is represented with the following equation: I ( $\mu A)=0.04+0.1273$  x [E2] with  $R^2=0.994.$  Furthermore, the limit of detection (LOD) and limit of quantification (LOQ) of the SPCE/Eu<sub>2</sub>O<sub>3</sub>@rGO sensor were evaluated by using Eqs. (7) and 8:

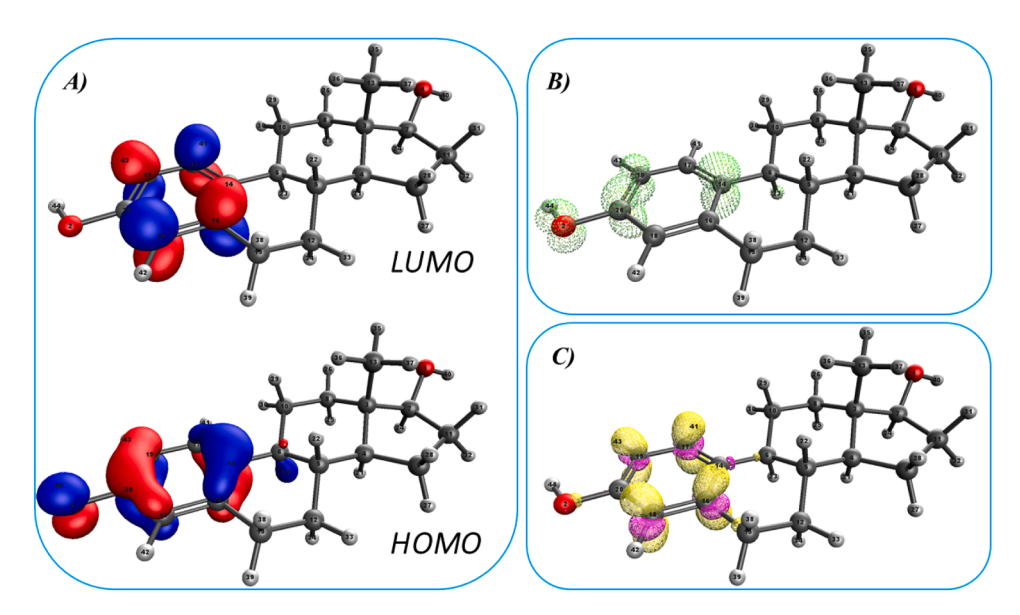


Fig. 4. A) HOMO and LUMO of E2; B) Electron (spin) density of E2 corresponding radical cation; C) Plot of the Fukui function towards nucleophilic  $(f_i^+)$  attack.

The main oxidation product

Scheme 1. Proposed oxidation mechanisms of E2, determined by DFT.

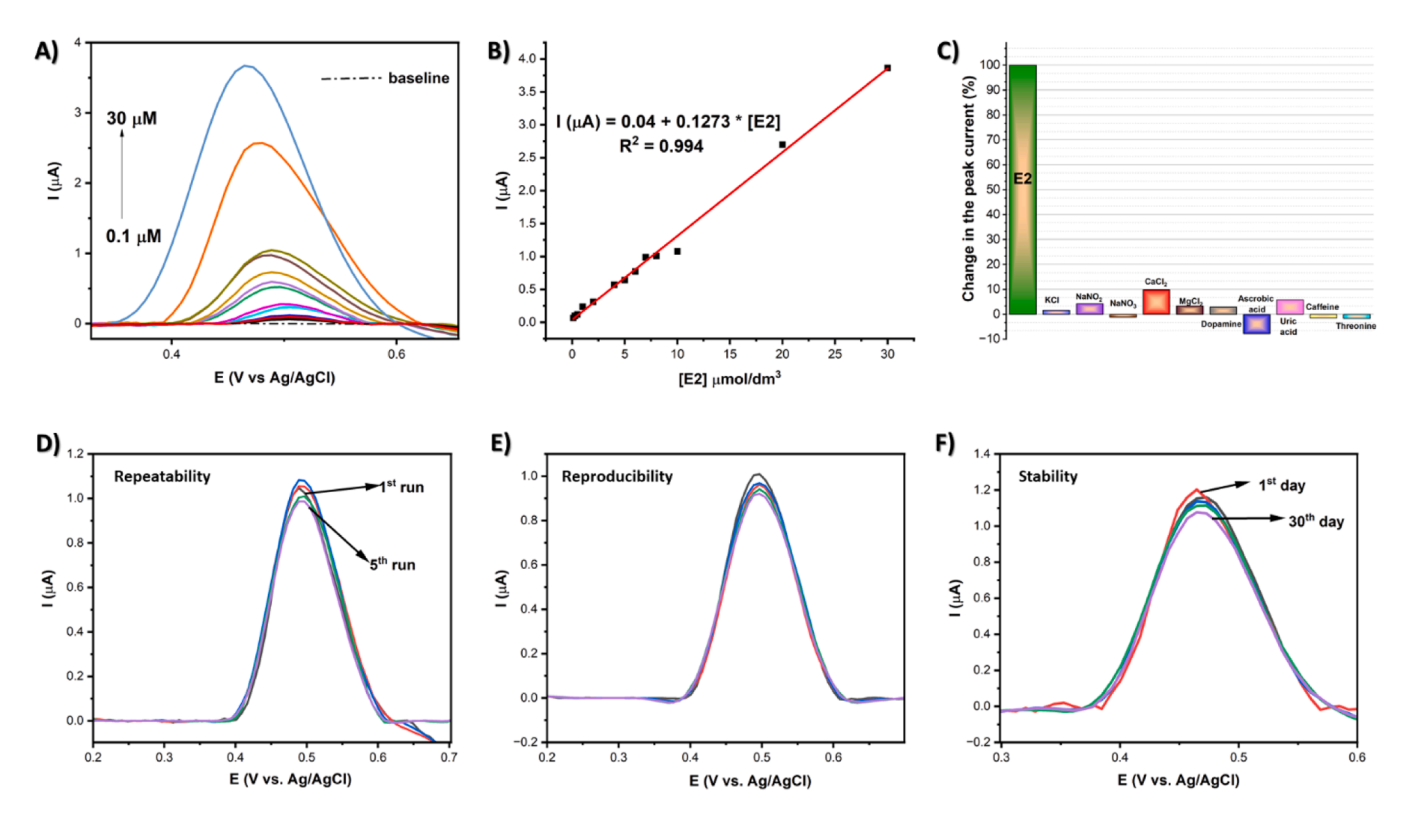


Fig. 5. A) SWV response of the SPCE/Eu<sub>2</sub>O<sub>3</sub>@rGO sensor with different concentrations of E2 (0.1–30  $\mu$ M) in BRBS (pH 4.0); B) A linear relationship between the oxidation peak currents and E2 concentrations; C) The bar graph of the relative inaccuracy (%) of current vs interfering molecules; D) SWV signal of five consecutive repeatability studies in the presence of 10  $\mu$ M E2; E) SWV signal of reproducibility study in the presence of 10  $\mu$ M E2; F) SWV indicates storage stability performance for 1–30 days in the presence of 10  $\mu$ M E2.

$$LOD = \frac{3 \times \delta}{s} \tag{7}$$

$$LOQ = \frac{10 \ x \ \delta}{s} \tag{8}$$

Where ' $\sigma$ ' represents the standard deviation of the blank signal and ' $\delta$ ' corresponds to the slope of the calibration curve. The fabricated SPCE/Eu<sub>2</sub>O<sub>3</sub>@rGO sensor demonstrated an impressive LOD of 0.06  $\mu$ M and a limit of quantification (LOQ) of 0.236  $\mu$ M. Additionally, the sensitivity,

calculated as the ratio of the slope to the electroactive surface area, was found to be 2.44  $\mu A~\mu M^{-1}~cm^{-2}$ . These findings confirm the exceptional sensing performance of the SPCE/Eu<sub>2</sub>O<sub>3</sub>@rGO sensor for E2 detection. Furthermore, the LOD and sensitivity were compared with previously reported results (Table 1), where the SPCE/Eu<sub>2</sub>O<sub>3</sub>@rGO sensor showed highly satisfactory performance in comparison.

The comparative analysis reveals that the sensor developed in this study demonstrates comparable or superior performance for the evaluated electroanalytical parameters. The proposed method and the SPCE/

Table 1
Comparative analytical performances of various electrochemical sensors for E2 detection.

Electrode	Technique	Linear range (µM)	LOD (nM)	Reference
G-ZnO/GCE	DPV	0.05-100	8.3	[40]
Pd/N-RGO/GCE	DPV	0.005 - 0.02	1.8	[41]
GNR/FS-Au-CA/CPE	DPV	0.1-50	7.4	[42]
RGO/CuTthP/GCE	DPV	0.1-10	5.3	[43]
Cu(LNO <sub>2</sub> ) <sub>2</sub> /rGO/	LSV	2-42	53	[44]
SPCE				
CBGC	DPV	0.15 - 3.5	92	[45]
Al <sub>2</sub> O <sub>3</sub> /GCE	LSV	0.4-40	80	[46]
RGO-DHP/GCE	LSV	0.4-10	77	[47]
Fe <sub>3</sub> O <sub>4</sub> NPs-BMI.PF6/ CPE	SWV	0.1–10	50	[48]
Eu <sub>2</sub> O <sub>3</sub> @rGO/ SPCE	SWV	0.1-30	60	This work

Eu<sub>2</sub>O<sub>3</sub>@rGO sensor stand out for their advantages, including the use of low-cost materials for nanocomposite synthesis, a straightforward synthesis process, rapid fabrication of working electrodes, and an ecofriendly approach. As the electrode preparation process does not involve the use of biological species such as antibodies or enzymes, the developed sensor offers significant stability and resistance to external condition needed for straightforward on-site sensing. Furthermore, it presents a promising opportunity for transitioning the proposed approach from laboratory research to commercial applications.

## 11. Impact of potential interfering substances on sensor performance

The selectivity of the proposed electrode of SPCE/Eu<sub>2</sub>O<sub>3</sub>@rGO was investigated by SWV in BRBS at pH 4. This selectivity study was performed in 10  $\mu M$  of E2 with ten times higher concentrations than different interfering compounds, generally present in real samples, which could potentially affect the sensor performance:  $Mg^{2+}, Na^+, K^+, NO_3, Ca^{2+}, Cu^2, NO_2, SO_4^2$ , ascorbic acid, dopamine, caffeine, threonine, and uric acid. After the addition of dopamine, ascorbic acid, and uric acid, due to their oxidation at similar potentials, a shift in the oxidation peak current was observed; however, the current value remained unaffected. Fig. 5C shows a change in the current signal of <10 % in the presence of interfering substances at concentrations ten times higher than that of the target analyte. The selectivity studies demonstrated that the oxidation current of E2 remained unaffected by any interfering species, highlighting the SPCE/Eu<sub>2</sub>O<sub>3</sub>@rGO sensor's exceptional selectivity for E2 detection.

## 11.1. Evaluating the repeatability, reproducibility, and storage stability of the proposed sensor

The reproducibility and repeatability of the SPCE/Eu<sub>2</sub>O<sub>3</sub>@rGO sensor were evaluated using the SWV method in BRBS (pH 4) containing 10 μM of E2. Repeatability was tested by performing five consecutive measurements with the same SPCE/Eu<sub>2</sub>O<sub>3</sub>@rGO sensor (Fig. 5D), yielding a relative standard deviation of 3.59 %. Similarly, reproducibility was assessed by fabricating five separate SPCE/Eu<sub>2</sub>O<sub>3</sub>@rGO sensors (Fig. 5E), resulting in a relative standard deviation of 3.46 %. The stability of the proposed sensor was further evaluated using SWV in the presence of 10 µM E2 at pH 4.0, throughout 1 to 30 days (specifically on the 1st, 7th, 10th, 15th, and 30th days), as illustrated in Fig. 5F. A relative standard deviation (RSD) of 4.06 % was obtained, confirming that the SPCE/Eu<sub>2</sub>O<sub>3</sub>@rGO sensor exhibits excellent storage stability. These results demonstrate the reliability and robustness of the SPCE/ Eu<sub>2</sub>O<sub>3</sub>@rGO sensor, emphasizing its potential as a promising nanocomposite for selective and sensitive E2 detection in real-world applications.

## 12. Real sample analysis

The developed SPCE/Eu<sub>2</sub>O<sub>3</sub>@rGO sensor was used to detect estradiol (E2) in tap water, river water, and saliva samples to demonstrate its practical applicability. The E2 content in these samples was analyzed using the proposed square wave voltammetry (SWV) method, with UV–Vis spectrometry employed as a validation technique. Three different E2 concentrations (5, 10, and 15  $\mu M$ ) were spiked into each sample. Based on the obtained voltammograms (Fig. 6A-D), peak current intensities, and calibration curves, the E2 concentrations were determined. These values were compared to the spiked concentrations, and recovery percentages were calculated (Table 2).

To further verify the method's accuracy, UV–Vis spectrometry was employed for E2 determination in the same samples (Figure S4 A-D). The results obtained with the SPCE/Eu<sub>2</sub>O<sub>3</sub>@rGO sensor closely matched those from the UV–Vis validation method, confirming the reliability and accuracy of the proposed approach (Table 2). Human saliva samples labeled as sample 1 and sample 2 exhibit slightly lower recovery values when spiked with 10  $\mu$ M, likely due to potential matrix effects. The results obtained with the SPCE/Eu<sub>2</sub>O<sub>3</sub>@rGO sensor closely matched those from the UV–Vis validation method, confirming the reliability and accuracy of the proposed approach (Table 2).

## Conclusion

In this work, ultrafine europium oxide particles were synthesized by the hydrothermal method, which were further used to form a composite with synthesized reduced graphene oxide. This achieved a synergistic effect of both nanomaterials, resulting in excellent electrocatalytic capabilities of the newly formed composite. The morphological characteristics examined using advanced spectroscopic methods indicated the uniform structure of the nanomaterial. Moreover, the electrochemical characteristics of the obtained composite showed outstanding results. Finally, the composite was used to modify a screen-printed carbon electrode, which showed excellent electrocatalytic capabilities toward detecting the endocrine disruptor estradiol. Enviable results were achieved in the analytical performance of the designed sensor, which showed a detection limit of only 0.06  $\mu M$  and a wide linear operating range from 1 to 30  $\mu$ M. Other parameters of the analytical method, such as repeatability (3.59 %), reproducibility (3.46 %), and stability (over 30 days), showed excellent results. When the sensor was used to monitor the concentration of estradiol in two different aqueous real water samples and two different human saliva samples, its excellent analytical performances were confirmed. Furthermore, a comprehensive quantum chemical analysis has been conducted to clarify the redox behavior of estradiol, offering a robust theoretical framework that supports the interpretation of experimental findings. Overall, the novel sensor is a promising analytical tool for routine estradiol detection and monitoring, with excellent predispositions for further modification towards disposable and point-of-need applications.

## CRediT authorship contribution statement

Aleksandar Mijajlović: Writing – original draft, Methodology, Conceptualization. Vesna Stanković: Writing – original draft, Methodology, Investigation, Conceptualization. Filip Vlahović: Writing – original draft, Methodology, Investigation, Conceptualization. Tijana Mutić: Writing – original draft, Methodology, Investigation, Conceptualization. Petar Ristivojević: Investigation. Nikolaos Argirusis: Investigation. Georgia Sourkouni: Methodology, Investigation, Conceptualization. Christos Argirusis: Methodology, Investigation, Conceptualization. Jasmina Vidić: Writing – original draft, Methodology, Investigation, Conceptualization, Conceptualization. Dalibor Stanković: Writing – review & editing, Writing – original draft, Supervision, Methodology, Conceptualization.

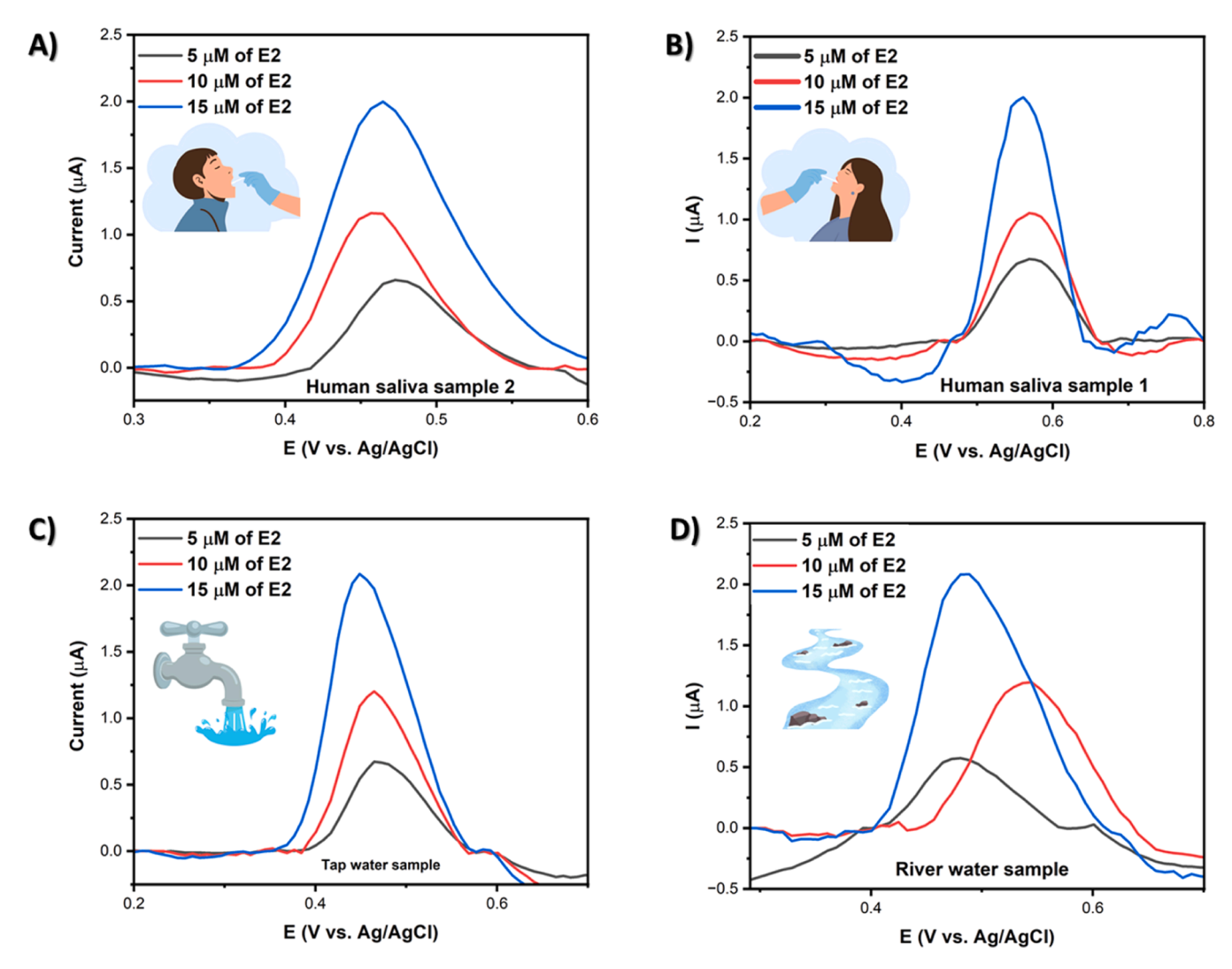


Fig. 6. SWV current response for E2 detection in A) saliva sample 1, B) saliva sample 2 C) tap water, D) river water over SPCE/Eu<sub>2</sub>O<sub>3</sub>@rGO developed sensor.

 $\label{table 2} \mbox{Results for E2 determination in spiked samples utilizing SPCE/Eu_2O_3@rGO sensor, using SWV method, and UV-Vis validation method.}$ 

Sample	Found (µM)	Added (μM)	Found (µM) SWV method	Recovery ( %)	Found (µM) UV–Vis method
Tap water	/	5	4.99	99.85	4.81
		10	9.12	91.25	10.39
		15	16.00	106.69	14.76
River water	/	5	4.56	91.2	4.97
		10	9.05	90.48	9.54
		15	16.09	107.26	15.03
Human	/	5	4.93	98.54	4.57
saliva		10	8.56	85.65	9.08
sample 1		15	15.35	102.37	15.03
Human	/	5	4.88	97.60	4.88
saliva		10	8.79	87.92	9.10
sample 2		15	15.37	102.51	14.83

## Declaration of competing interest

The authors declare that they have no known competing financial interests or personal relationships that could have appeared to influence the work reported in this paper.

## Acknowledgements

This research has been financially supported by the European Union, MOBILES (Monitoring and detection of biotic and abiotic pollutants by electronic, plants and microorganisms based sensors), Grant Agreement 101135402, https://doi.org/10.3030/101135402, and the Ministry of Science, Technological Development and Innovation of Republic of Serbia (Contract No: 451–03–66/2024–03/200026 and 451–03–136/2025–03/200168).

## Supplementary materials

Supplementary material associated with this article can be found, in the online version, at doi:10.1016/j.electacta.2025.146913.

## Data availability

No data was used for the research described in the article.

## References

- Franck Mauvais-Jarvis, Deborah J. Clegg, Andrea L. Hevener, The role of estrogens in control of energy balance and glucose homeostasis, Endocr. Rev. 34 (3) (2013) 309–338, https://doi.org/10.1210/er.2012-1055.
- [2] Seema Patel, Ahmad Homaei, Akondi Butchi Raju, Biswa Ranjan Meher, Estrogen: the necessary evil for Human health, and ways to tame it, Biomed. PharmacOther 102 (2018) 403–411, https://doi.org/10.1016/j.biopha.2018.03.078.

- [3] Susanna C Larsson, Siddhartha Kar, John R B Perry, Paul Carter, Mathew Vithayathil, Amy M Mason, Douglas F Easton, Stephen Burgess, Serum estradiol and 20 site-specific cancers in women: mendelian randomization study, J. Clin. Endocrinol. Metab. 107 (2) (2022) e467–e474, https://doi.org/10.1210/ clinem/deab713
- [4] Concetta Pironti, Maria Ricciardi, Antonio Proto, Pietro Massimiliano Bianco, Luigi Montano, Oriana Motta, Endocrine-disrupting compounds: an overview on their occurrence in the aquatic environment and Human exposure, Water 13 (10) (2021) 1347, https://doi.org/10.3390/w13101347.
- [5] Phumudzo Budeli, Mutshiene Deogratias Ekwanzala, John Onolame Unuofin, Maggy Ndombo Benteke Momba, Endocrine disruptive estrogens in wastewater: revisiting bacterial degradation and zymoremediation, Environ. Technol. Innov. 21 (2021) 101248, https://doi.org/10.1016/j.eti.2020.101248.
- [6] Marinella Farré, Marina Kuster, Rikke Brix, Fernando Rubio, María-J.López De Alda, Damià Barceló, Comparative study of an estradiol enzyme-linked immunosorbent assay kit, liquid chromatography-Tandem mass spectrometry, and Ultra performance liquid chromatography-Quadrupole time of flight mass spectrometry for part-per-trillion analysis of estrogens in water samples, J. Chromatogr. A 1160 (1–2) (2007) 166–175, https://doi.org/10.1016/j. chroma.2007.05.032.
- [7] Auwal M. Musa, Janice Kiely, Richard Luxton, Kevin C. Honeychurch, Recent progress in screen-printed electrochemical sensors and biosensors for the detection of estrogens, TrAC Trends Anal. Chem. 139 (2021) 116254, https://doi.org/ 10.1016/j.trac.2021.116254.
- [8] Yen-Yi Lee, Balasubramanian Sriram, Sea-Fue Wang, Sakthivel Kogularasu, Guo-Ping Chang-Chien, A comprehensive review on emerging role of rare earth oxides in electrochemical biosensors, Microchem. J. 193 (2023) 109140, https://doi.org/10.1016/j.microc.2023.109140.
- [9] Nur Azizah Ferdiana, Husein Hernandi Bahti, Dikdik Kurnia, Santhy Wyantuti, Synthesis, characterization, and electrochemical properties of rare earth element nanoparticles and its application in electrochemical nanosensor for the detection of various biomolecules and hazardous compounds: a review, Sens. Biosensing. Res. 41 (2023) 100573. https://doi.org/10.1016/j.jsbsr.2023.100573.
- [10] Aleksandar Mijajlović, Miloš Ognjanović, Dragan Manojlović, Filip Vlahović, Slađana Đurđić, Vesna Stanković, Dalibor Stanković, Eu2O3@Cr2O3 Nanoparticles-modified carbon paste electrode for efficient electrochemical sensing of neurotransmitters precursor I.-DOPA, Biosens. (Basel) 13 (2) (2023) 201, https://doi.org/10.3390/bios13020201.
- [11] Jingjing Jiang, Xinyi Lin, Dong Ding, Guowang Diao, Graphitic-phase carbon nitride-based electrochemiluminescence sensing analyses: recent advances and perspectives, RSC. Adv. 8 (35) (2018) 19369–19380, https://doi.org/10.1039/ C8RA02221F.
- [12] Yen-Yi Lee, Balasubramanian Sriram, Sea-Fue Wang, Sakthivel Kogularasu, Guo-Ping Chang-Chien, A comprehensive review on emerging role of rare earth oxides in electrochemical biosensors, Microchem. J. 193 (2023) 109140, https://doi.org/10.1016/j.microc.2023.109140.
- [13] Min Wei, Liang Qiao, Hanguang Zhang, Stavros Karakalos, Kuo Ma, Zheng Fu, Mark T. Swihart, Gang Wu, Engineering reduced graphene oxides with enhanced electrochemical properties through multiple-step reductions, Electrochim. Acta 258 (2017) 735–743, https://doi.org/10.1016/ji.electacta.2017.11.120.
- [14] Gloria Ebube Uwaya, Praveen Kumar Sappidi, Krishna Bisetty, Development of a Co<sub>3</sub> O<sub>4</sub> /rGO modified electrochemical sensor for highly sensitive riboflavin detection, ChemElectroChem. 11 (15) (2024), https://doi.org/10.1002/ celc.202400290 e202400290.
- [15] Hao-Xin Mai, Ling-Dong Sun, Ya-Wen Zhang, Rui Si, Wei Feng, Hong-Peng Zhang, Hai-Chao Liu, Chun-Hua Yan, Shape-selective synthesis and oxygen storage behavior of Ceria nanopolyhedra, nanorods, and nanocubes, J. Phys. Chem. B 109 (51) (2005) 24380–24385, https://doi.org/10.1021/jp055584b.
- [16] Lisong Chen, Xiangzhi Cui, Yongxia Wang, Min Wang, Ruihao Qiu, Zhu Shu, Lingxia Zhang, et al., One-step synthesis of sulfur doped graphene foam for oxygen reduction reactions, Dalton. Trans. 43 (9) (2014) 3420, https://doi.org/10.1039/c3dt52553a
- [17] Bilal Yilmaz, Yucel Kadioglu, Determination of 17 β-estradiol in pharmaceutical preparation by UV spectrophotometry and high performance liquid chromatography methods, Arab. J. Chem. 10 (2017) S1422–S1428, https://doi. org/10.1016/j.arabjc.2013.04.018.
- [18] Chuanen Guo, Chengxiang Wang, Hongyan Sun, Dongmei Dai, Hongtao Gao, A simple electrochemical sensor based on rGO/MoS<sub>2</sub> /CS modified GCE for highly sensitive detection of Pb(n) in tobacco leaves, RSC. Adv. 11 (47) (2021) 29590–29597, https://doi.org/10.1039/D1RA05350G.
- [19] T.R. Poorani, C. Ramya, M. Ramya, Effect of topo ratio in the formation of In-situ hydrophobic core–Shell nanoparticle of europium oxide, J. Inorg. Organomet. Polym. Mater. 33 (11) (2023) 3413–3440, https://doi.org/10.1007/s10904-023-02779-6
- [20] Hemarani Annadurai, Renganathan Vengudusamy, Shen-Ming Chen, Yu-Hsin Lin, Yuan-Han Ku, C.R. Kao, Sonochemical assisted europium(III) oxide-Graphiticcarbon nitride nanocomposite for reversible electrochemical detection of quinol, J. Electrochem. Soc. 171 (9) (2024) 097520, https://doi.org/10.1149/1945-7111/ ad790b.
- [21] Ruspika Sundaresan, Vinitha Mariyappan, Tse-Wei Chen, Shen-Ming Chen, Muthumariappan Akilarasan, Xiaoheng Liu, Jaysan Yu, One-dimensional rareearth tungstate nanostructure encapsulated reduced graphene oxide electrocatalyst-based electrochemical sensor for the detection of organophosphorus pesticide, J. Nanostructure Chem. 14 (5) (2024) 355–368, https://doi.org/ 10.1007/s40097-023-00524-6.

- [22] Brian Roehrich, Lior Sepunaru, Impedimetric measurement of exchange currents and ionic diffusion coefficients in individual pseudocapacitive nanoparticles, ACS. Meas. Sci. Au 4 (4) (2024) 467–474, https://doi.org/10.1021/ acsmeasurescian.4c00017
- [23] Alan P. Brown, Fred C. Anson, Electron transfer kinetics with both reactant and product attached to the electrode surface, J. Electroanal. Chem. Interfacial. Electrochem. 92 (2) (1978) 133–145, https://doi.org/10.1016/S0022-0728(78) 80174-0
- [24] Junhua Li, Jianbo Jiang, Dan Zhao, Zhifeng Xu, Mengqin Liu, Peihong Deng, Xing Liu, Chumming Yang, Dong Qian, Haobin Xie, Facile synthesis of Pd/N-doped reduced graphene oxide via a moderate wet-chemical route for non-enzymatic electrochemical detection of estradiol, J. Alloys. Compd. 769 (2018) 566–575, https://doi.org/10.1016/j.jallcom.2018.08.016.
- [25] Ali Özcan, Duygu Topçuoğulları, Voltammetric determination of 17-β-estradiol by cysteamine self-assembled gold nanoparticle modified fumed silica decorated graphene nanoribbon nanocomposite, Sens. Actuators B: Chem. 250 (2017) 85–90, https://doi.org/10.1016/j.snb.2017.04.131.
- [26] Fernando C. Moraes, Bruno Rossi, Maria C. Donatoni, Kleber T.De Oliveira, Ernesto C. Pereira, Sensitive determination of 17β-estradiol in river water using a graphene based electrochemical sensor, Anal. Chim. Acta 881 (2015) 37–43, https://doi.org/10.1016/j.aca.2015.04.043.
- [27] E. Laviron, General expression of the linear potential sweep voltammogram in the case of diffusionless electrochemical systems, J. Electroanal. Chem. Interfacial. Electrochem. 101 (1) (1979) 19–28, https://doi.org/10.1016/S0022-0728(79) 80075-3.
- [28] M.J. Frisch, G.W. Trucks, H.B. Schlegel, G.E. Scuseria, M.A. Robb, J.R. Cheeseman, G. Scalmani, V. Barone, G.A. Petersson, H. Nakatsuji, X. Li, M. Caricato, A. Marenich, J. Bloino, B.G. Janesko, R. Gomperts, B. Mennucci, H.P. Hratchian, J. V. Ortiz, A.F. Izmaylov, J.L. Sonnenberg, D. Williams-Young, F. Ding, F. Lipparini, F. Egidi, J. Goings, B. Peng, A. Petrone, T. Henderson, D. Ranasinghe, V. G. Zakrzewski, J. Gao, N. Rega, G. Zheng, W. Liang, M. Hada, M. Ehara, K. Toyota, R. Fukuda, J. Hasegawa, M. Ishida, T. Nakajima, Y. Honda, O. Kitao, H. Nakai, T. Vreven, K. Throssell, J.A. Montgomery Jr., J.E. Peralta, F. Ogliaro, M. Bearpark, J.J. Heyd, E. Brothers, K.N. Kudin, V.N. Staroverov, T. Keith, R. Kobayashi, J. Normand, K. Raghavachari, A. Rendell, J.C. Burant, S.S. Iyengar, J. Tomasi, M. Cossi, J.M. Millam, M. Klene, C. Adamo, R. Cammi, J.W. Ochterski, R.L. Martin, K. Morokuma, O. Farkas, J.B. Foresman, D.J. Fox, Gaussian 09, Revision A.O2, Gaussian, Inc., Wallingford CT, 2016.
- [29] W. Koch, M.C. Holthausen, A Chemist's Guide to Density Functional Theory, Wiley, 2015.
- [30] R.G. Parr, Y. Weitao, Density-Functional Theory of Atoms and Molecules, Oxford University Press, 1994.
- [31] C. Lee, W. Yang, R.G. Parr, Development of the Colle-Salvetti correlation-energy formula into a functional of the electron density, Phys. Rev. B 37 (2) (1988) 785–789, https://doi.org/10.1103/PhysRevB.37.785.
- [32] A.D. Becke, A new mixing of Hartree-Fock and local density-functional theories, J. Chem. Phys. 98 (2) (1993) 1372–1377, https://doi.org/10.1063/1.464304.
- [33] H. Kruse, S. Grimme, A geometrical correction for the inter- and intra-molecular basis set superposition error in Hartree-Fock and density functional theory calculations for large systems, J. Chem. Phys. 136 (15) (2012), https://doi.org/ 10.1063/1.3700154.
- [34] A.V. Marenich, C.J. Cramer, D.G. Truhlar, Universal solvation model based on solute electron density and on a continuum model of the solvent defined by the bulk dielectric constant and atomic surface tensions, J. Phys. Chem. B 113 (18) (2009) 6378–6396, https://doi.org/10.1021/jp810292n.
- [35] R.G. Parr, W. Yang, Density functional approach to the frontier-electron theory of chemical reactivity, J. Am. Chem. Soc. 106 (14) (1984) 4049–4050, https://doi. org/10.1021/ia00326a036
- [36] Ankit Kumar Singh, Shreanshi Agrahari, Ravindra Kumar Gautam, Ida Tiwari, Fabrication of an innovative electrochemical sensor based on graphene-coated silver nanoparticles decorated over graphitic carbon nitride for efficient determination of estradiol, Environ. Sci. Pollut. Res. 31 (27) (October 8, 2022) 38628–38644, https://doi.org/10.1007/s11356-022-23410-0.
- [37] Enock G. Arthur, Hana Ali, Armeen Hussain, Glen D. O'Neil, Square-wave voltammetry enables measurement of light-activated oxidations and reductions on n-type semiconductor/metal junction light-addressable electrochemical sensors, Anal. Chem. 95 (24) (2023) 9219–9226, https://doi.org/10.1021/acs. analchem.3c00630.
- [38] Aleksandar Mijajlović, Miloš Ognjanović, Vesna Stanković, Tijana Mutić, Slađana Đurđić, Branka B. Petković, Dalibor M. Stanković, A practical approach to triclosan detection: a novel Y2O3@GCN-modified carbon paste electrode for sensitive and selective detection in environmental and consumer products, Chemosensors 12 (12) (2024) 272, https://doi.org/10.3390/ chemosensors12120272.
- [39] Miriam M Ngundi, Omowunmi A Sadik, Takashi Yamaguchi, Shin-ichiro Suye, First comparative reaction mechanisms of β-estradiol and selected environmental hormones in a redox environment, Electrochem. commun. 5 (1) (2003) 61–67, https://doi.org/10.1016/S1388-2481(02)00538-6.
- [40] Yali Jiang, Yuning Song, Jiyu Yu, Chao Tong, Electrochemical detection platform based on graphene-zinc oxide composite nanomaterials for 17β-estradiol determination in milk, Alex. Eng. J. 100 (2024) 170–175, https://doi.org/ 10.1016/j.aej.2024.05.047.
- [41] Junhua Li, Jianbo Jiang, Dan Zhao, Zhifeng Xu, Mengqin Liu, Peihong Deng, Xing Liu, Chunming Yang, Dong Qian, Haobin Xie, Facile synthesis of Pd/N-doped reduced graphene oxide via a moderate wet-chemical route for non-enzymatic

- [42] Ali Özcan, Duygu Topçuoğulları, Voltammetric determination of 17-β-estradiol by cysteamine self-assembled gold nanoparticle modified fumed silica decorated graphene nanoribbon nanocomposite, Sens. Actuators B: Chem. 250 (2017) 85–90, https://doi.org/10.1016/j.snb.2017.04.131.
- [43] Fernando C. Moraes, Bruno Rossi, Maria C. Donatoni, Kleber T.De Oliveira, Ernesto C. Pereira, Sensitive determination of 17β-estradiol in river water using a graphene based electrochemical sensor, Anal. Chim. Acta 881 (2015) 37–43, https://doi.org/ 10.1016/j.aca.2015.04.043.
- [44] Claudia Núñez, Ronald Nelson, Gerald Tabilo, Paulina Pefaur, Rodrigo Castillo, Alifhers Mestra, Simultaneous detection of serotonin and 17β-estradiol using rGO/ SPCE modified with Cu(II) complex: a novel approach for PMDD diagnosis, Chemosensors 12 (8) (2024) 164, https://doi.org/10.3390/ chemosensors12080164.
- [45] Joanna Smajdor, Robert Piech, Martyna Ławrywianiec, Beata Paczosa-Bator, Glassy carbon electrode modified with carbon black for sensitive estradiol determination by means of voltammetry and flow injection analysis with amperometric detection, Anal. Biochem. 544 (2018) 7–12, https://doi.org/ 10.1016/j.ab.2017.12.025.
- [46] Qiong He, Shuai Yuan, Cuie Chen, Shengshui Hu, Electrochemical properties of estradiol at glassy carbon electrode modified with nano-Al2O3 film, Mater. Sci. Eng.: C 23 (5) (2003) 621–625, https://doi.org/10.1016/S0928-4931(03)00053-5.
- [47] Bruno C. Janegitz, Fabrício A.Dos Santos, Ronaldo C. Faria, Valtencir Zucolotto, Electrochemical determination of estradiol using a thin film containing reduced graphene oxide and dihexadecylphosphate, Mater. Sci. Eng.: C 37 (2014) 14–19, https://doi.org/10.1016/j.msec.2013.12.026.
- [48] Fernanda Moreira, Edson Roberto Santana, Almir Spinelli, Ionic liquid-supported magnetite nanoparticles as electrode modifier materials for estrogens sensing, Sci. Rep. 10 (1) (2020) 1955, https://doi.org/10.1038/s41598-020-58931-6.